Bremsstrahlung from tritium β decay

B. Budick, Jiansheng Chen, and Hong Lin
Physics Department, New York University, New York, New York 10003
(Received 31 January 1992)

Both external and internal bremsstrahlung produced in the β decay of tritium and of tritium-rare gas mixtures have been investigated. The ratio of external to internal bremsstrahlung varied for the different sources by more than two orders of magnitude. From an analysis of the shape of the x-ray spectrum, the maximum kinetic energy of electrons emitted in the β decay of tritium molecules has been determined to be 18 556(6) eV.

PACS number(s): 23.40.−s, 27.10.+h, 13.40.Ks

I. INTRODUCTION

The bremsstrahlung that is emitted in tritium β decay is of two types: internal bremsstrahlung (IB) that results from the creation of the fast moving electron, and external bremsstrahlung (EB) as the electron decelerates in the surrounding material. In either case, the end point of the resulting photon spectrum is equal to the end point of the electron's energy distribution. Indeed, a new measurement of the atomic mass difference between ^{3}H and ^{3}He based on the bremsstrahlung spectrum has been published [1]. This novel approach to the mass difference would not have been possible without a thorough investigation of the systematic effects that can modify the photon spectrum. The results of that investigation are presented in this paper.

However, there are other purposes for which this study should be valuable. A high resolution experiment on the end point of the EB spectrum has been suggested as a means of measuring the mass of the electron antineutrino [2]. Alternatively, if the IB spectrum could be isolated, it could better serve the same purpose since its shape can be predicted with greater confidence. In this experiment, by changing the surrounding material in which the EB occurs, the EB/IB ratio could be varied by more than two orders of magnitude.

Bremsstrahlung from low energy electrons plays an important role in astrophysics [3] and in plasma physics [4]. Workers in these disciplines employ approximations to describe the thick-target bremsstrahlung they observe. This paper addresses itself to the adequacy of those approximations.

In the present work, electrons from tritium decay were completely stopped in glass bulbs containing mixtures of tritium and the rare gases neon, argon, or xenon. One bulb with initially pure tritium was also studied. A lithium-drifted silicon detector recorded the bremsstrahlung x-ray spectrum.

II. THEORY OF THE EXPERIMENT

The photon spectrum for IB can be expressed as [5]

$$\mathrm{IB} = \frac{\alpha G^2 M^2}{4\pi^4}\frac{1}{k}g(k)\ \text{photons/sec MeV},$$

where G is the weak-coupling constant, M is the matrix element between initial and final states, k is the photon energy in units of $m_e c^2$, $g(k)$ is the spectral function, and α is the fine structure constant.

To evaluate the EB spectrum, we require knowledge of the thick-target bremsstrahlung function $I(E,k,Z)$, which describes the photon spectrum that is emitted when electrons of initial kinetic energy E stop in a particular radiator of atomic number Z. The EB spectrum from an allowed β decay is obtained by convoluting $I(E,k,Z)$ with the well-known Fermi shape

$$N(W)\,dW = F(Z_d,W)\,W\,(W_0 - W)^2\sqrt{W^2-1}\,dW,$$

where $F(Z_d,W)$ is the Fermi function, and Z_d is the atomic number of the daughter nucleus, W_0 is the total energy available for the decay which depends somewhat on the atomic or molecular environment of the decaying triton, because the ^{3}He daughter may have a different distribution of final states in different hosts [6]. For our purposes, the Fermi function can be taken as

$$F(Z_d,W) = \frac{2\pi\eta}{1-e^{-2\pi\eta}}\,, \qquad \eta = \frac{Z_d e^2}{\hbar v}\,,$$

where v denotes the velocity of the electron far from the nucleus.

The photon spectrum for EB can be expressed as

$$\mathrm{EB} = \frac{G^2M^2}{2\pi^3}\frac{1}{k}f(k,Z)\ \text{photons/sec MeV},$$

where

$$f(k,Z) = \int_{1+k}^{W_0} I(E,k,Z)N(W)\,dW \tag{1}$$

is the spectral distribution for EB, and $E = W - 1$ in units of $m_e c^2$.

A commonly employed approximation for the thick-target bremsstrahlung function is Kramers' formula [7]

$$I_{\mathrm{Kr}}(E,k,Z) = 2CZ(E-k)\,, \tag{2}$$

where C is a proportionality constant independent of photon energy, but which may depend weakly on the kinetic energy of the electron. Its approximate value for purposes of comparing EB to IB is 1.4×10^{-3} MeV^{-1}. It

TABLE I. Bremsstrahlung distributions and the absorption corrections for the sample of $0.7\,^3H_2 + 0.3$ Xe. Columns two and three list values of the spectral functions (in arbitrary units) at several photon energies for IB and EB (calculated with I_{Kr}), which are independent of the gas mixture. Column four gives values of the spectral function for EB corresponding to I_{thick}. Self-absorption and glass absorption are listed in columns five and six, and the comparisons between the contributions to EB from the gas mixture, the glass wall, and from the secondary bremsstrahlung are shown in the last two columns.

Photon energy k (keV)	Spectral IB $g(k)$	Spectral EB $f_{Kr}(k)$	Spectral EB $f_{thick}(k)$	Self-absorption correction	Glass absorption correction	S_{glass}/S_{gas} (%)	S_{2nd}/S_{gas} (%)
6	11.3	8.01	7.97	0.22	8.8×10^{-5}	1.6	6.6
8	5.27	4.19	4.16	0.32	1.7×10^{-2}	1.1	0.027
10	2.10	1.88	1.86	0.40	0.12	0.90	
12	0.663	0.677	0.659	0.45	0.29	0.70	
14	0.140	0.164	0.158	0.48	0.45	0.49	
16	0.0125	0.0168	0.0160	0.50	0.58	0.27	
18	0.000 032	0.000 039	0.000 037	0.51	0.68	0.058	

follows that

$$\frac{EB}{IB} = 1.2Z\,\frac{f_{Kr}(k)}{g(k)}\,, \tag{3}$$

where

$$f_{Kr}(k) = \frac{1}{2CZ}\int_{1+k}^{W_0} I_{Kr}(E,k,Z)N(W)\,dW = \int_{1+k}^{W_0}(W-1-k)N(W)\,dW\,.$$

Values for the two spectral functions at several photon energies are listed in Table I. Their ratio is of order unity in the range of interest in this study, 5–18 keV. Thus, the ratio of EB to IB depends strongly on the choice of radiator. An experiment that emphasizes high bremsstrahlung rates, such as the neutrino mass determination using EB mentioned above, would employ a high Z radiator. However, if one seeks to avoid possible systematic errors associated with thick-target bremsstrahlung, one would choose a low Z radiator to enhance IB.

III. THICK-TARGET BREMSSTRAHLUNG

The review article by Koch and Motz [8] summarizes much of the early work on thick-target bremsstrahlung. In discussing Kramers' formula [Eq. (2)], the authors stress the assumptions in Kramers' semiclassical derivation: the thin-target bremsstrahlung distribution is independent of photon energy, the energy loss is proportional to Z/E (the Thomson-Whiddington law), and the electrons slow down continuously. Kramers recognized that in comparing his formula with experiment, corrections for electron backscattering from the target as well as for photon absorption would be required.

It is worth noting that a distribution identical to Kramers' formula was obtained in a quantum mechanical calculation by Kirkpatrick [9]. Kirkpatrick used the Sommerfeld nonrelativistic theory for the thin-target distribution and semiempirical values for the collisional energy loss. Kirkpatrick's formula serves as the basis for the excellent discussion of thick-target bremsstrahlung given by Evans [10].

On the experimental side, Storm [11] compared Kramers' formula with experimental results for electrons with energies of 12, 30, 60, 100, 200, and 300 keV stopping in tungsten. In addition, he calculated thick-target spectra based on Sommerfeld's thin-target distribution, as well as on thin-target distributions derived by Heitler using the Born approximation. For electron energies below 100 keV, and after correcting for electron backscattering and for photon attenuation, Storm found good agreement between experiment and each of the above theoretical approaches.

Thick-target spectra for electrons in the range 10–30 keV impinging on targets of Al, Cu, Mo, and W were measured by Chervenak and Liuzzi [12]. They compared their results with Kramers' formula and found that for photons with $k > E/2$ (for which photon attenuation corrections can be made most reliably), the spectra do resemble straight lines. On the other hand, their results obtained by integrating over photon energy for the total energy emitted imply that C is not a constant independent of initial electron energy E.

In the present study, the thick-target bremsstrahlung function was derived from the thin-target distribution by means of the relation

$$I_{thick}(E,k,Z) = \int_{E'>k}^{E} I_{thin}(E',k,Z)\left(\frac{dE'}{-dE'/dx}\right), \tag{4}$$

where dE/dx is the mean electron energy loss per unit path length. Berger and Seltzer recently calculated reliable values for dE/dx [13] and for $I_{thin}(E,k,Z)$ [14]. These authors kindly supplied values for both quantities for small steps in E and k. Smooth spline function fits to their points were used as inputs in Eq. (4). The resultant $I_{thick}(E,k,Z)$ was stored in a computer and ultimately folded with the β spectrum as in Eq. (1). To compare with $f_{Kr}(k)$, values for the corresponding spectral function

$$f_{thick}(k) = \frac{1}{2CZ}\int_{1+k}^{W_0} I_{thick}(E,k,Z)N(W)\,dW$$

are listed in Tables I–V.

TABLE II. Bremsstrahlung distributions and the absorption corrections for the sample of $0.5\,^3H_2 + 0.5\,Xe$.

Photon energy k (keV)	Spectral EB $f_{thick}(k)$	Self-absorption correction	Glass absorption correction	S_{glass}/S_{gas} (%)	S_{2nd}/S_{gas} (%)
6	8.33	0.17	7.8×10^{-5}	1.5	7.2
8	4.34	0.27	1.6×10^{-2}	0.98	0.028
10	1.93	0.35	0.12	0.76	
12	0.685	0.40	0.28	0.57	
14	0.164	0.44	0.45	0.39	
16	0.016 6	0.46	0.58	0.21	
18	0.000 038	0.48	0.68	0.045	

TABLE III. Bremsstrahlung distributions and the absorption corrections for the sample of $0.5\,^3H_2 + 0.5\,Ar$.

Photon energy k (keV)	Spectral EB $f_{thick}(k)$	Self-absorption correction	Glass absorption correction	S_{glass}/S_{gas} (%)	S_{2nd}/S_{gas} (%)
6	7.87	0.42	2.3×10^{-4}	4.6	2.2
8	3.91	0.47	2.6×10^{-1}	4.4	0.017
10	1.68	0.49	0.15	4.0	
12	0.577	0.51	0.33	3.3	
14	0.134	0.51	0.49	2.5	
16	0.013 2	0.51	0.61	1.4	
18	0.000 030	0.52	0.71	0.30	

TABLE IV. Bremsstrahlung distributions and the absorption corrections for the sample of $0.5\,^3H_2 + 0.5\,Ne$.

Photon energy k (keV)	Spectral EB $f_{thick}(k)$	Self-absorption correction	Glass absorption correction	S_{glass}/S_{gas} (%)	S_{2nd}/S_{gas} (%)
6	7.27	0.54	7.6×10^{-4}	7.0	0.64
8	3.49	0.55	4.4×10^{-2}	7.0	0.010
10	1.47	0.55	0.20	6.5	
12	0.493	0.55	0.38	5.6	
14	0.113	0.55	0.54	4.3	
16	0.011 0	0.55	0.66	2.6	
18	0.000 024	0.55	0.74	0.54	

TABLE V. Bremsstrahlung distributions and the absorption corrections for the pure $^3H_2$ sample.

Photon energy k (keV)	Spectral EB $f_{thick}(k)$	Self-absorption correction	Glass absorption correction	S_{glass}/S_{gas} (%)	S_{2nd}/S_{gas} (%)
6	3.56	0.53	1.1×10^{-3}	17.6	0.41
8	1.49	0.53	5.1×10^{-2}	19.6	0.008
10	0.549	0.53	0.21	20.7	
12	0.161	0.53	0.40	20.3	
14	0.0316	0.53	0.56	17.7	
16	0.002 55	0.53	0.67	12.2	
18	0.000 004	0.53	0.75	2.56	

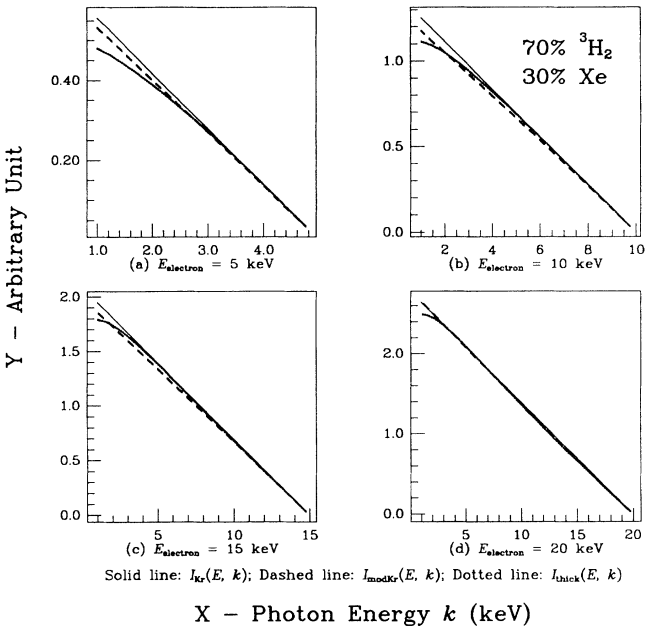

FIG. 1. Comparison between different forms of the thick-target bremsstrahlung function at four electron energies for a mixture of 70% $^3H_2$ and 30% Xe.

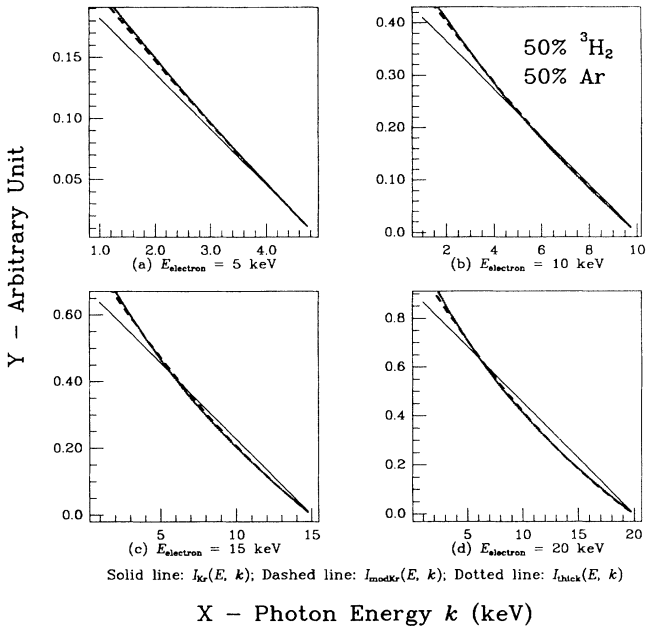

FIG. 3. Same as Fig. 1, but for a mixture of 50% $^3H_2$ and 50% Ar.

For purposes of comparison with Kramers' formula, $I_{\text{thick}}(E, k, Z)$ calculated in this manner was approximated in a modified form:

$$I_{\text{modKr}}(E, k, Z) = 2CZ\left[(1 - aE)(E - k) + (b + cE)(E - k)^2\right] ,$$

where a, b, and c are small correction constants. In Fig. 1, the photon spectrum for electrons of 5, 10, 15, and 20 eV stopping in a 70:30 tritium:xenon sample are compared for I_{Kr}, I_{modKr}, and I_{thick}. All three are in reasonable agreement for the higher energy photons. The agreement becomes poorer for lower energy photons at lower electron energies. Similar behavior is noted for electrons stopping in 50:50 mixtures of tritium and xenon, tritium and argon, and tritium and neon as shown in Figs. 2–4.

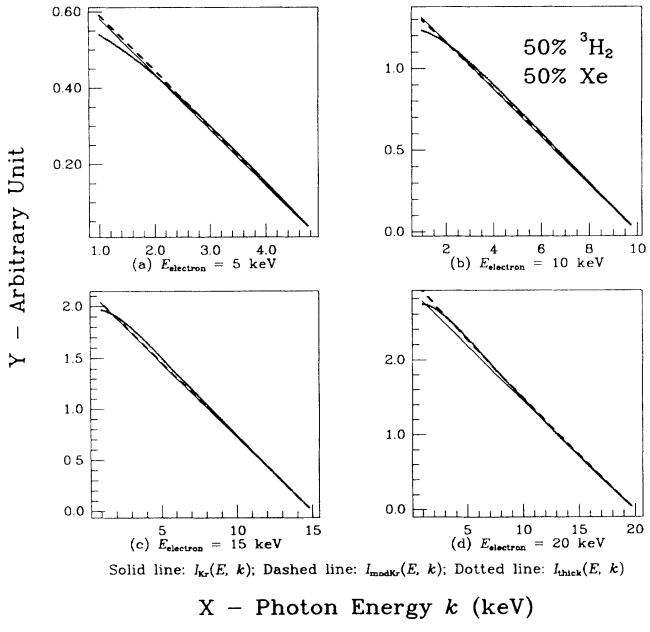

FIG. 2. Same as Fig. 1, but for a mixture of 50% $^3H_2$ and 50% Xe.

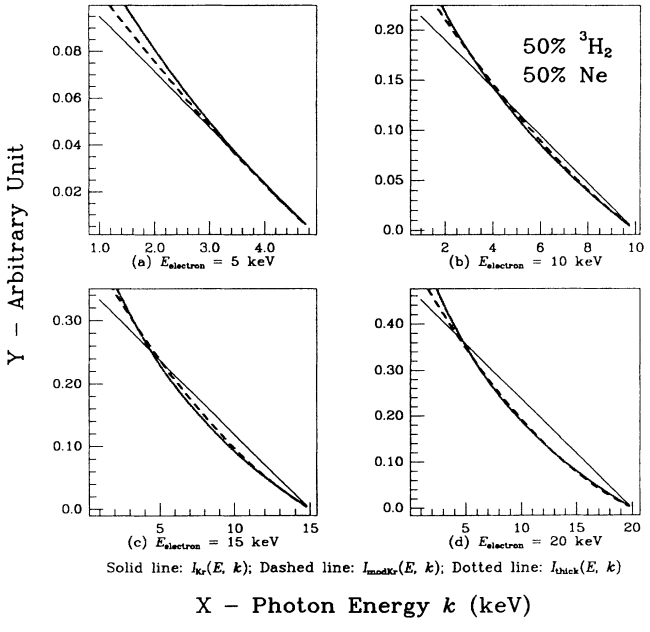

FIG. 4. Same as Fig. 1, but for a mixture of 50% $^3H_2$ and 50% Ne.

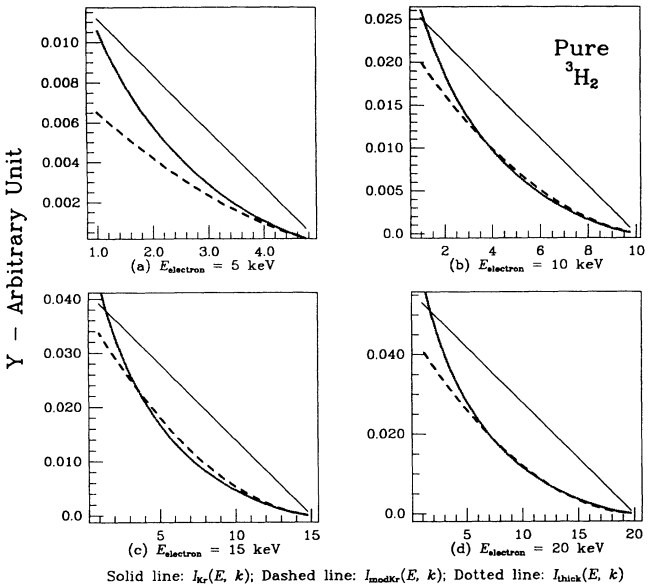

FIG. 5. Same as Fig. 1, but for pure $^3H_2$.

For electrons stopping in pure tritium, use of the unmodified Kramers' form would lead to serious error (see Fig. 5).

The primary reason for the excellent agreement of I_{Kr} with the more accurately calculated thick-target distributions in the $^3H_2$-Xe mixtures is that the thin-target bremsstrahlung cross section for 15 and 20 keV electrons in Xe is fortuitously flat as a function of photon energy in accord with Kramers' first assumption. This is not true for the other mixtures or for pure tritium.

IV. METHODS AND PROCEDURES

A. Sources

Pure tritium gas or mixtures of tritium with rare gases were contained in glass bulbs approximately 1 cm^3 in volume. The glass is Corning 1720, which has a permeation rate for helium of 2 $\times 10^{-16}$ cm^3/sec cm^2 (area) mm (thickness) cm (Hg pressure difference) at room temperature [15]. The permeation rate for hydrogen is lower by roughly two orders of magnitude. (The permeation rate is the product of the diffusion constant and the solubility.) The bulbs were blown at New York University. A preliminary value for the wall thickness of each bulb was determined by measuring the attenuation of Np L x rays at 11.9, 13.9, and 17.8 keV. Attenuation coefficients could be calculated based on the known composition of the 1720 glass. A method for deriving a more precise value for the bulb thicknesses was found during the data analysis as described below. The bulbs were then leak tested, baked out, and shipped under vacuum to Amersham Corporation in England for filling.

The compositions of the filling mixtures in atomic percent of tritium to xenon were 70:30 and 50:50 for the first two bulbs, and they contained 2.8 and 1.9 Ci of tritium initially. The remaining three bulbs contained mixtures of 50:50 tritium:argon, 50:50 tritium:neon, and pure tritium. Based on the permeation rates for 1720 glass given above, after one half-life, less than 0.2 ppm of the tritium will have leaked out, while the leakage of the ^{3}He daughter will be roughly an order of magnitude greater. Upon receipt from Amersham, the bulbs were tested for tritium leakage using a sensitive tritium sniffer. The sniffer was calibrated immediately prior to testing with a 3.7 μCi ^{133}Xe source. An upper limit on the leakage rate of 0.5 μCi per half-life was determined for each of the bulbs.

As mentioned above, the rare gas in each bulb served to enhance the EB rate over that of IB in accord with Eq. (3). In addition, the rare gas served a second important function. For a pure tritium sample, the EB rate will change as the tritium is replaced by ^{3}He simply because the radiative and nonradiative stopping powers are greater for ^{3}He than for ^{3}H. One may estimate the magnitude of this effect by using the effective Z for a mixture [10],

$$Z_{\text{eff}} = \frac{N_1 Z_1^2 + N_2 Z_2^2 + N_3 Z_3^2 + \cdots}{N_1 Z_1 + N_2 Z_2 + N_3 Z_3 + \cdots},$$

where N_i is the number of atoms/cm^3 of the ith component. The conclusion from this approach is that the change in the EB rate due to $^3\text{H} \rightarrow {}^3\text{He}$ conversion will be less than 0.2% over a two year period if initially $N_{^3H_2} = N_{\text{Xe}}$, for example.

The above remarks are predicated on tritium *not* sticking to the walls of the glass bulbs. If the tritium stuck to the glass, a significant number of electrons would radiate in the glass which would alter Z_{eff} dramatically. This, in turn, would affect both the shape of spectrum (by modifying the ratio of EB to IB) and the half-life. We measured the half-life and obtained a result that agrees closely with other experiments [16]. Our analysis of the spectrum shape is also consistent with no sticking. Nonetheless, some electrons emitted close to the wall do radiate in the glass. Their effect is considered below in the Results section.

B. Detector

The filtered bremsstrahlung spectrum extends from about 5 to 18.6 keV. This range is ideal for the 3 mm thick Si(Li) detector used in this experiment. Energy and efficiency calibration were carried out automatically each day by positioning an ^{241}Am source in front of the detector. Augmented by fluorescence from Pb and Cd, the range of x and γ radiation from this source extends from 10.5 to 26.4 keV. The tail-to-peak ratio as a function of photon energy was determined with the help of ^{55}Fe, ^{99}Tc^m, and ^{109}Cd sources. The slight decrease in detector efficiency above 16 keV was measured by determining the $K\alpha/K\beta$ ratios for carrier-free samples of ^{99}Tc^m and ^{109}Cd, and from the intensity ratios of the Np L x rays emitted by the ^{241}Am source. These same sources were employed to determine that the detector

resolution (FWHM) increased from 185 eV at 5.9 keV to 285 eV at 18.6 keV.

With modest shielding, the background in the small-volume detector was only 50 events in each 16 eV interval per year. This is the typical dispersion, 16 eV/channel, used in data acquisition. The overall linearity of the detection system was checked with x rays and γ rays from ^{55}Fe, ^{57}Co, ^{99}Tc^{m}, ^{109}Cd, and ^{241}Am.

C. Data acquisition

Data acquisition was controlled by an IBM PC. When data collection in a Canberra 35^{+} multichannel analyzer was complete, it signalled the PC, which then recorded the spectrum on a hard disk and sent a signal to a microprocessor that was programmed to step a SLO-SYN motor coupled to a precision lead screw. The motor positioned another tritium sample or the calibration source in front of the detector with a reproducibility of 2×10^{-4} cm.

Pulses from the Si(Li) preamplifier were amplified by a Canberra 2020. This amplifier was chosen for its pileup rejection capability. Dead-time and pileup rejection inefficiencies were measured as a function of counting rate. Together, they amounted to 2.1% for the highest counting rates encountered in our experiment, 1100 Hz.

V. RESULTS

A typical bremsstrahlung spectrum for a tritium-xenon mixture is shown in Fig. 6. However, before the observed spectrum can be compared with predictions, the calculated spectrum must be corrected for absorption in the gas and in the glass of each bulb. Both corrections were made by carefully summing the photon intensities reaching the detector from all points in the gas volume and from the glass walls. Final values for the bulb thickness were obtained by leaving the thickness as one of the three free parameters when fitting the observed spectrum. These corrections are listed in Tables I–V. In all cases, attenuation in the glass predominates.

Two other corrections required consideration. The first is for the finite source size effect. Not all the electrons stop in the gas mixture. Some radiate while stopping in the glass. From the known geometry of each bulb, and the value of dE/dx for the mixture it contained, the fractions of photons radiated in the gas mixture and in the glass were calculated at each photon energy. Results of these calculations for all the bulbs are also listed in Tables I–V to illustrate the magnitude of the finite source size effect. As anticipated, the effect is greatest for low energy photons and for the lighter gas mixtures, especially for pure tritium.

The second correction is due to secondary bremsstrahlung from the glass. Photons absorbed in the glass create photoelectrons, primarily from the K and L shells of the elements composing the glass. These photoelectrons emit their own EB. This contribution to the total spectrum for each of the five bulbs at different photon energies is listed in the final column in Tables I–V. The effect is significant only for pure tritium at the lowest photon energies.

These corrections, along with the detector resolution, were folded into the calculated spectrum and compared with the observed spectrum. Three parameters in the calculated spectrum were varied to improve the fit: the amplitude and end point of the spectrum, and the thickness of the bulb. A variation in the end point primarily shifts the spectrum horizontally, while a change in the bulb thickness mainly affects the amplitude.

In order to deduce the EB/IB ratio, each spectrum was fit over a large region to include photons below 12 keV where IB makes its most significant contribution (see Table I). The fit for the mixture of 70% $^{3}H_2$ and 30% Xe is the smooth curve shown in Fig. 6. The fits for the remaining four bulbs are shown in Figs. 7–10. As noted above, the identified sources of systematic error are largest in the case of the pure tritium sample at low photon energies. This may explain why the data points in Fig. 10

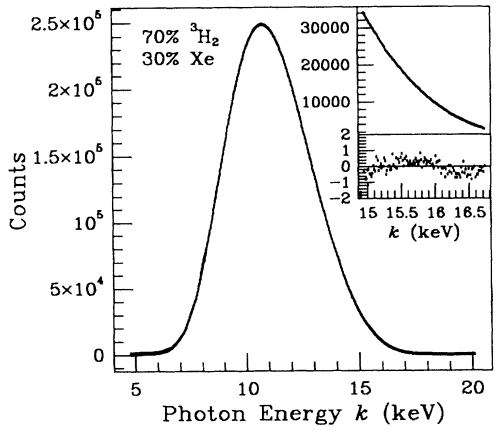

FIG. 6. Filtered bremsstrahlung spectrum from a mixture of 70% $^{3}H_2$ and 30% Xe. The solid line is a fit to the data points. Inset: The fit and the residuals in the high energy region.

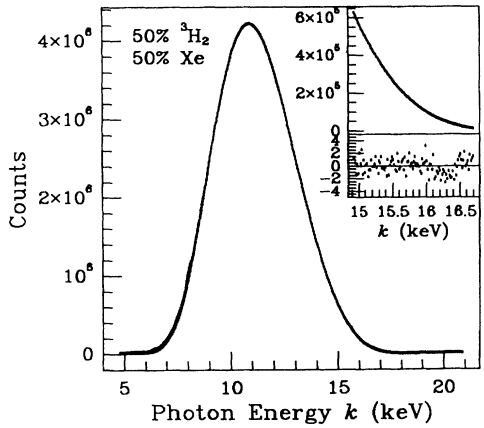

FIG. 7. Same as Fig. 6, but for a mixture of 50% $^{3}H_2$ and 50% Xe.

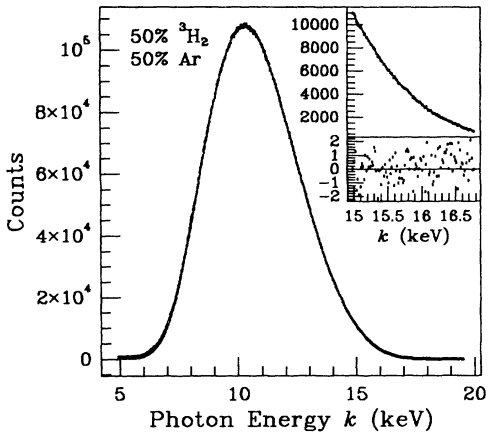

FIG. 8. Same as Fig. 6, but for a mixture of 50% $^3H_2$ and 50% Ar.

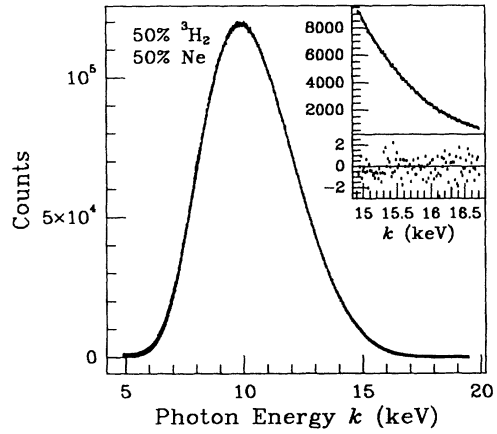

FIG. 9. Same as Fig. 6, but for a mixture of 50% $^3H_2$ and 50% Ne.

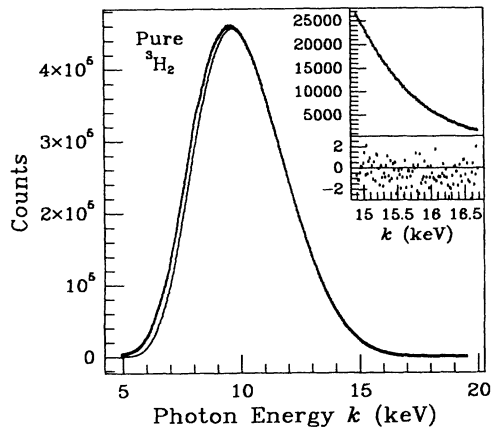

FIG. 10. Same as Fig. 6, but for pure $^3H_2$.

are above the predicted curve at energies below 10 keV. In each figure, the inset shows the fit and the residuals in the 15–17 keV region from which the end-point values may be derived with high precision. The residuals for the first two samples, Figs. 6 and 7, indicate that there are systematic deviations in the fit. However, the residuals in Fig. 6 for the mixture of 70% $^3H_2$ and 30% Xe are considerably smaller than those in Fig. 7 for the mixture of 50% $^3H_2$ and 50% Xe (note the change in the vertical scale). These deviations are discussed below.

VI. DISCUSSION

In Table VI are presented the χ^2 values for the fits to each of the observed spectra both for the larger energy region, 10–17 keV, and for the restricted high energy region, 15–17 keV, shown in the insets. It is apparent that the known sources of systematic error have been adequately accounted for, and that unknown sources must be small. The last column lists the maximum photon energy determined for each bulb. See Ref. [1] for a discussion of the statistical and systematic errors that contribute to the uncertainty in this result.

In deducing a weighted average value for the end-point energy, the result for the 50:50 tritium-xenon mixture was excluded. The high χ^2 value for this sample is a consequence of the large residuals which also show systematic deviations from the fit. It is directly attributable to a visible nonuniformity in the glass thickness immediately facing the detector that is very difficult to model and correct for. The bulb containing this mixture has the largest fitted thickness parameter, a reflection of its nonuniformity. The residuals in Fig. 6 may have a similar cause since the bulb containing the 70:30 tritium-xenon mixture has the second largest fitted thickness parameter. Both of these bulbs belonged to the first batch fabricated by our glass blower. With the 50:50 tritium-xenon mixture excluded, the end-point energy based on the remaining four samples is measured as 18 556(6) eV.

The observed EB/IB ratio at the photon energy of 10 keV for each of the bulbs is also listed in Table VI. It has not been corrected for the finite source size effect and is essentially what would be measured for an infinite source. The ratios for the mixtures are in good qualitative agreement with expectations based on Eq. (3). Predicted ratios are 54, 58, 18, 10, and 0.31, respectively. For all of the mixtures, the spectral functions, $f_{\text{thick}}(k)$ and $g(k)$, are of the same magnitude at 10 keV. Therefore, EB/IB is mainly a function of Z of the radiator. However, for pure tritium, Kramers' formula fails badly (see Fig. 5). Indeed, the ratio of the spectral functions at 10 keV is roughly 1/4, and decreases at higher energies. This, combined with the low Z of the radiator, is responsible for the dominance of IB in the pure tritium spectrum. It is important to note that the end point energy is not very sensitive to the EB/IB ratio. A change in the EB/IB ratio of 20% shifts the end point by less than 2 eV, primarily because the functions $f(k)$ and $g(k)$ have slopes in the 15–17 keV region that are the same to within 1%.

TABLE VI. Characteristics of the gas samples used in the experiment are given in the first six columns. The goodness of fit and the deduced end point are listed in the last three columns.

Gas mixture	Bulb thickness (mm)	Counting rate (Hz)	Bulb radius (cm)	Pile-up (%)	EB/IB (10 keV)	χ^2/d.f. (15–17 keV)	χ^2/d.f. (10–17 keV)	End point (keV)
$0.7\,^3H_2 + 0.3$ Xe	0.392	910	0.79	0.28	45(5)	1.07	1.04	18.551(10)
$0.5\,^3H_2 + 0.5$ Xe	0.408	516	0.64	0.16	59(6)	1.68	2.07	18.565(21)
$0.5\,^3H_2 + 0.5$ Ar	0.359	71	0.62	0.017	32(3)	1.04	1.09	18.560(12)
$0.5\,^3H_2 + 0.5$ Ne	0.310	81	0.79	0.016	15(2)	1.06	1.14	18.548(12)
$^3H_2$	0.294	78	0.65	0.013	0.29(3)	1.18	1.26	18.560(11)

For the case of a low-energy-allowed β transition, such as that of tritium, one further simple test is possible to illuminate the adequacy of Kramers' formula for EB in the end-point region. For this purpose, the Fermi function can be expressed as [17]

$$F(Z_d, W) = 1 + \frac{\pi\alpha Z_d W}{\sqrt{W^2 - 1}} . \tag{5}$$

Higher-order terms distort the shape of the spectrum by less than 0.4%. In the Appendix, it is shown that the integral in Eq. (1) can then be expanded in a Taylor's series about the end point using Leibnitz' Rule. The leading terms are

$$f(k, Z) = \frac{2CZ}{12}(W_0 - 1 - k)^4 \times \left(W_0\sqrt{W_0^2 - 1} + \pi\alpha Z_d W_0^2 \right) .$$

$W_0 - 1$ is the electron's kinetic energy in units of the electron's rest mass energy. A Kurie-type plot can be constructed by plotting the fourth-root of $k\times$EB versus k.

Such a plot is shown in Fig. 11 for the mixture of 70% $^3H_2$ and 30% Xe, where the fourth root of the predicted spectrum is plotted as a solid line, and the points are the fourth roots of the raw data points. The predicted spectrum includes the detector resolution and the attenuation in the glass wall. Thus, both spectra deviate slightly from the straight-line behavior at the lower photon energies where attenuation in the glass becomes important. At energies near the end point, the detector resolution distorts the straight-line behavior. Nonetheless, the adequacy of the fourth-root approximation is apparent. For Xe, as noted above, Kramers' formula is a reasonable approximation, while the other systematic effects, including IB, are small, and were not included. The significance of the excellent fit is primarily that it, along with the detailed fits obtained above, confirms our analysis of the shape and intensity of EB.

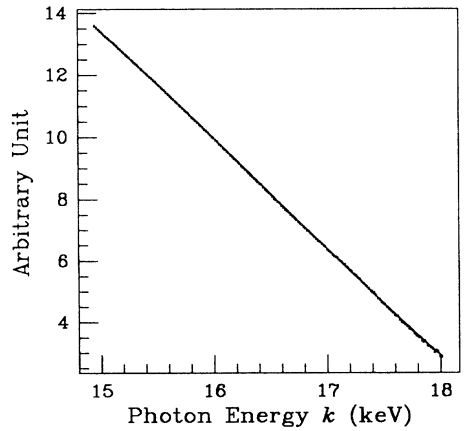

FIG. 11. Kurie-type plot in the high energy region for the mixture of 70% $^3H_2$ and 30% Xe. The points and the solid line are the fourth roots of the raw data points and the predicted spectrum attenuated by the glass, respectively.

Finally, we considered the effect of using the theoretical values for $I_{\text{thin}}(E', k, Z)$ on the EB spectrum, and, more significantly, on the end-point determination. Berger and Seltzer estimate the uncertainty in their calculated values of I_{thin} as 10%, and in dE'/dx as 5% for the photons and electrons in our energy range. Accordingly, we varied the *slope* of the thin-target bremsstrahlung cross section by 15%. The shift in the end point was roughly 2 eV.

VII. CONCLUSION

A systematic study has been carried out of bremsstrahlung from low-energy electrons emitted in tritium β decay. The tritium was mixed with rare gases that served as radiators to enhance the contribution of external bremsstrahlung. For a pure tritium sample, internal bremsstrahlung was responsible for most of the observed x rays. Indeed, it was possible to vary the EB/IB ratio by more than two orders of magnitude. A thorough investigation of thick-target bremsstrahlung was required to fit the data from all the different radiators. In addition, systematic effects that could distort the photon spectrum, such as finite source size and secondary bremsstrahlung, were studied for each of the samples. The good agreement obtained between predicted and observed spectra indicates that tritium bremsstrahlung may serve as a useful tool to investigate other features connected with tritium β decay, e.g., the ^{3}H-^{3}He atomic mass difference.

ACKNOWLEDGMENTS

The authors gratefully acknowledge valuable assistance provided by M. J. Berger and S. M. Seltzer. This work

was supported in part by the National Science Foundation under Grant No. PHY-8500520.

APPENDIX

Writing Kramers' formula as

$$I_{\rm Kr} = 2CZ(W-1-k)\,,$$

where $W-1$ is the electron's kinetic energy, and using Eq. (5) as the Fermi function, the integral in Eq. (1) is a linear combination of

$$\int_{1+k}^{W_0} (W-1-k)W^n(W_0-W)^2(W^2-1)^{\frac{2-n}{2}}\,dW\,,$$

where $n=1$ corresponds to the first term in Eq. (5), and $n=2$ the second term. For the end-point region, $k \to E_0 = W_0 - 1$, and the appropriate variable is $\alpha = E_0 - k$. Letting $x = E - k = W - 1 - k$, the integral becomes

$$F(\alpha) = \int_0^\alpha f(x,\alpha)\,dx\,,$$

with

$$f(x,\alpha) = (x-\alpha+W_0)^n(\alpha-x)^2 \times x\left[(x-\alpha+W_0)^2-1\right]^{\frac{2-n}{2}}\,.$$

The expansion about $\alpha = 0$ follows from a Taylor's series,

$$F(\alpha) = F|_{\alpha=0} + \left.\frac{dF}{d\alpha}\right|_{\alpha=0}\alpha + \frac{1}{2}\left.\frac{d^2F}{d\alpha^2}\right|_{\alpha=0}\alpha^2 + \frac{1}{6}\left.\frac{d^3F}{d\alpha^3}\right|_{\alpha=0}\alpha^3 + \cdots\,.$$

Leibnitz's Rule for differentiating an integral with respect to the upper limit of integration is

$$\frac{dF}{d\alpha} = \int_0^\alpha \frac{\partial f}{\partial\alpha}\,dx + f|_{x=\alpha}\,.$$

Hence,

$$\frac{d^2F}{d\alpha^2} = \int_0^\alpha \frac{\partial^2 f}{\partial\alpha^2}\,dx + \left.\frac{\partial f}{\partial\alpha}\right|_{x=\alpha} + \frac{d}{d\alpha}(f|_{x=\alpha})\,,$$

$$\frac{d^3F}{d\alpha^3} = \int_0^\alpha \frac{\partial^3 f}{\partial\alpha^3}\,dx + \left.\frac{\partial^2 f}{\partial\alpha^2}\right|_{x=\alpha} + \frac{d}{d\alpha}\left(\left.\frac{\partial f}{\partial\alpha}\right|_{x=\alpha}\right) + \frac{d^2}{d\alpha^2}(f|_{x=\alpha})\,,$$

$$\cdots\cdots\,.$$

It is easy to show that, when x is equal to α, the first nonvanishing partial derivative is

$$\left.\frac{\partial^2 f}{\partial\alpha^2}\right|_{x=\alpha} = 2\alpha W_0^n(W_0^2-1)^{\frac{2-n}{2}}\,.$$

This, together with each of the integrals, vanishes when α is equal to zero. The first nonvanishing contribution to the Taylor's series comes from

$$\left.\frac{d^4F}{d\alpha^4}\right|_{\alpha=0} = \left.\frac{d}{d\alpha}\left(\left.\frac{\partial^2 f}{\partial\alpha^2}\right|_{x=\alpha}\right)\right|_{\alpha=0} = 2W_0^n(W_0^2-1)^{\frac{2-n}{2}}\,.$$

Thus,

$$F = \frac{1}{4!}\,2(W_0^2-1)^{\frac{2-n}{2}}\,\alpha^4 = \frac{1}{12}(E_0-k)^4\,W_0^n(W_0^2-1)^{\frac{2-n}{2}}\,.$$

[1] B. Budick, Jiansheng Chen, and Hong Lin, Phys. Rev. Lett. **67**, 2626 (1991).
[2] G. L. Borchert, D. Gotta, H. R. Koch, R. Salziger, H. J. Probst, and O. W. B. Schult, Nucl. Instrum. Methods Phys. Res. **A174**, 507 (1989).
[3] J. C. Brown and A. L. MacKinnon, Astrophys. J. Lett. **292**, 31 (1985).
[4] G. H. McCall, J. Phys. D **15**, 823 (1982).
[5] C. S. Wang Chang and D. L. Falkoff, Phys. Rev. **76**, 365 (1949).
[6] B. Budick, Phys. Rev. Lett. **51**, 1034 (1983).
[7] H. A. Kramers, Philos. Mag. **46**, 836 (1923).
[8] H. W. Koch and J. W. Motz, Rev. Mod. Phys. **31**, 921 (1959).
[9] P. Kirkpatrick, Phys. Rev. **70**, 446 (1946).
[10] Robley D. Evans, *The Atomic Nucleus* (McGraw-Hill, New York, 1955).
[11] Ellery Storm, Phys. Rev. A **5**, 2328 (1972).
[12] J. G. Chervenak and A. Liuzzi, Phys. Rev. A **12**, 26 (1985).
[13] M. J. Berger and S. M. Seltzer, *Stopping Powers and Ranges of Electrons and Positrons*, 2nd Ed., Nat. Bur. Stand., Report No. NBSIR 82-2550-A, 1983.
[14] S. M. Seltzer and M. J. Berger, At. Data Nucl. Data Tables **35**, 345 (1986).
[15] V. O. Altemose, J. Appl. Phys. **32**, 1309 (1961).
[16] B. Budick, Jiansheng Chen, and Hong Lin, Phys. Rev. Lett. **67**, 2630 (1991).
[17] D. H. Wilkinson, Nucl. Phys. **A377**, 474 (1982).